Int J Adv Manuf Technol (2014) 75:1177–1187
DOI 10.1007/s00170-014-6202-z

ORIGINAL ARTICLE

Mechanistic approach for prediction of forces in micro-drilling of plain and glass-reinforced epoxy sheets

I. Rahamathullah · M. S. Shunmugam

Received: 20 November 2012 / Accepted: 23 July 2014 / Published online: 15 August 2014

Abstract Aerospace and automobile industries extensively use components made of plastics and fiber-reinforced plastics which require micro-machining operations including micro-drilling to be carried out. Various attempts are reported in the literature to study different strategies and model the forces in micro-drilling with a view to produce micro-holes having large aspect ratio and to reduce drill breakage. The force models are more statistical than mechanistic in approach. In the present work, an attempt is made to develop mechanistic models of thrust and torque in micro-drilling of plain epoxy sheets. Material model capturing strain rate and temperature-dependent yield strength of epoxy material and basic principles of machining are employed for this purpose. The mechanistic model for prediction of thrust and torque is validated using well-planned full factorial design of experiments. Experiments are carried out using a carbide drill of 0.5-mm diameter with three levels for speed and feed on a high-speed miniature machine tool specially developed at the laboratory. The material model is extended to glass-reinforced plastics (GRP), and drilling forces are predicted using the proposed mechanistic model. In both cases of plain and GRP sheets, the model predictions are close to the experimentally measured drilling forces.

Keywords Micro-drilling · Epoxy · Glass reinforced · Mechanistic model · Thrust force · Torque

I. Rahamathullah
Department of Mechanical Engineering, Government College of Engineering, Bargur 635104, India

M. S. Shunmugam (✉)
Department of Mechanical Engineering, Indian Institute of Technology Madras, Chennai 600036, India
e-mail: shun@iitm.ac.in

Nomenclature **Drill geometry and cutting parameters**

R	Drill radius (mm)
$2W$	Web thickness (mm)
L	Lip length (mm)
r_e	Edge radius (mm)
δ	Helix angle (deg)
ρ	Semi-point angle (°)
ψ	Chisel edge angle (°)
s	Feed (mm/rev)
n	Spindle speed (rpm)

Cutting elements and relevant conditions

Δr	Elemental radial width on cutting lip/chisel edge (mm)
r	Distance from center of the drill to mid-point of the element chosen on lip/chisel edge (mm)
ΔL	Elemental lip width on lip (mm)
V	Velocity at the cutting element (mm/s)
ω	Web angle (°)
i	Inclination angle (°)
ν	Velocity angle (°)
t_0	Uncut chip thickness (mm)
$t_{\lim}$	Limiting uncut chip thickness (mm)
α_{ref}	Reference rake angle at the cutting element (°)
α_n	Rake angle at cutting element (°)
β_n	Friction angle at cutting element (°)
φ_n	Shear angle at cutting element (°)
η	Chip flow angle (°)
$\dot{\varepsilon}$	Strain rate in cutting (s^{-1})
α_f	Feed angle (°)
ϕ	Slip line field angle (°)
R_a	Indentation zone radius
C	Merchant's machining constant
τ	Shear strength of work material (MPa)

f_P, f_Q, f_R	Elemental forces per unit radial width along cutting, thrust and radial directions respectively (N/mm)
f_{pc}, f_{qc}, f_{rc}	Cutting force coefficients (MPa)
f_{pe}, f_{qe}, f_{re}	Edge force coefficients (MPa/mm)
Thru_j, Tang_j, Thru_{lip}	Elemental thrust and tangential forces with reference to drill axis (N)
Thru_{chi}, Thru_{ind}, Torq_{lip}	Thrust at cutting lips, chisel edge, and indentation zone (N)
Torq_{chi}, Torq_{ind}	Torque at cutting lips, chisel edge, and indentation zone (N mm)
Thru	Thrust force on the drill (N)
Torq	Torque on the drill (N mm)

Material property

σ_y	Compressive yield stress of the material (MPa)
$\sigma_i(0)$	Internal yield stress of the material at 0 K (MPa)
n_c	Material parameter to characterize the cooperative movement of the chain segments
h	The primary shear zone thickness (mm)
$\dot{\varepsilon}$	Process strain rate (s^{-1}) (computed for machining conditions)
$\dot{\varepsilon}_0$	Pre-exponential strain rate (s^{-1})
ΔH_β	β Activation energy (KJ/mol)
m	Material constant
V_a	Activation volume (m^3)
k	Boltzmann's constant (m^2 kg/s^2 K)
T	Absolute temperature (K)
τ_{comp}, τ_{fib}, τ_{mat}	Shear strength of composites, fiber, and matrix, respectively
v_{fib}, v_{mat}	Volume fraction of fiber and matrix, respectively

1 Introduction

Plastics and fiber-reinforced plastics are widely used in automotive and aerospace industries, as these materials offer considerable weight reduction and replace metals and alloys that find place in different components. The components made of these plastics also require additional machining operations, particularly for making holes for functional and assembly purposes. With miniaturization of features on the components, they are subject to micro-machining operations that include micro-drilling as well. Even though micro-drilling is carried out with drills having diameter less than 1.00 mm, drilling of holes with diameter 500 μm and below is considered to fall into the category of micro-drilling [1].

Literature survey presented here covers research work carried out in macro- and micro-drilling, with emphasis on plastics and fiber-reinforced plastics as work materials. Since many attempts to study drilling of the plastics and fiber-reinforced plastics have some kind of dependence on drilling of metals, it is not out of place to present a brief review of macro- and micro-drilling of metals first to understand the context. In case of twist drill, two types of elements are involved in metal removal [2, 3]. Drill lips form primary elements which have higher cutting velocity in comparison with secondary element. The secondary element is chisel edge of the drill which removes metal by cutting where the velocity is high enough as well as by extruding the metal at the center (referred to as indentation zone) where the cutting velocity is near 0.

A study on the mechanism of metal removal in macro-drilling and cutting forces has led to the development of statistical as well as mechanistic models [4]. The statistical models use regression techniques to develop the equations in which the coefficients represent influence of cutting parameters on the cutting forces [5]. The mechanistic models for cutting forces are strictly based on fundamental mechanical properties, while some mechanistic approaches evaluate a set of coefficients which have functional significance in determining the cutting forces. It is interesting to note that mechanistic approaches use oblique cutting principles which are extended from orthogonal cutting [6, 7].

Micro-drills not only differ from macro-drills in terms of size but also have higher ratio of chisel edge to diameter and appreciable cutting edge radius which influences the cutting phenomenon. Some manufacturers of micro-drills do not provide land or margin on them. It can be seen from the literature that approaches for modeling macro-drilling are extended to micro-drilling also. Mechanistic approach in modeling of cutting forces in micro-drilling has been reported by Gong and Ehmaan [8], and the cutting coefficients are evaluated from drilling experiments that are carried out using a 3.175-mm drill with a pilot hole slightly larger than the chisel edge. The cutting coefficients thus obtained are also used to predict forces acting on the cutting lips as well as the chisel edge. Being meso-scale drilling of metals, the material strengthening due to size effect [9] and role of cutting edge radius [10] do not come into picture.

In an earlier work carried out by Rao et al. in 1964, an attempt has been made to carry out a fundamental study of machining characteristics of plastics using orthogonal cutting experiments similar to those carried out on metals [11]. Machining studies on plastics have been well documented by Kobayashi [12]. It is interesting to note that studies on orthogonal edge cutting of unidirectional fiber-reinforced laminate have been carried out with different orientation of fibers [13–15]. However, drilling is carried out on the surface of the laminate, and the conditions encountered by the cutting edges of the drill are different. Most of the work reported in the literature on macro-drilling of plastics and fiber-reinforced plastics deal with study of hole quality and cutting forces involved [16–19]. A mechanistic approach for predicting cutting forces in drilling of fiber-reinforced composites is reported by Chandrasekharan et al. [20]. It is also mentioned in their paper that the material in the indentation zone is subjected compressive fracture instead of getting extruded like metals. The literature on micro-drilling of plastics and fiber-reinforced plastics is quite limited. Though hole quality in micro-drilling of fiber-reinforced plastics has been reported, the models for predicting the drilling forces are statistical in nature [21, 22]. In developing mechanistic model for micro-drilling of plastics, size effect in metals commonly attributed to geometrically necessary dislocation densities cannot be applied.

In the present work, plain and glass-reinforced epoxy sheets are taken as work materials to carry out micro-drilling studies. First, a mechanistic model is developed for plain epoxy sheet to predict the thrust and torque in micro-drilling, considering material removal in cutting lip, chisel edge, and indentation zones. The model is validated by conducting experiments with solid carbide drill of 0.5-mm diameter. The mechanistic model is next extended to cover glass-reinforced epoxy sheet, and the results are compared with experimentally measured drilling forces.

2 Mechanistic model

Basic studies in machining are carried out by orthogonal cutting which represents a cutting action with a single sharp edge placed perpendicular to the direction of cutting. This is a two-dimensional case with forces acting in a plane. Actual machining operations such as drilling and milling are multi-point cutting operations, and they very rarely satisfy orthogonal cutting conditions. In order to study these operations, principles of orthogonal cutting are extended to oblique cutting and then the investigations are carried out. Also, to develop mechanistic model of cutting forces, one has to capture the material behavior as cutting involves very high strains, strain rates, and temperatures as well as model the cutting action of different elements of the tool used. In case of a drill, two different elements, namely cutting lip and chisel edge, have to be considered. Micro-drills often have diameter less than 0.5 mm with ratio of chisel edge to diameter being large in comparison with that of macro-drills, and cutting edge radius in micro-drill plays a significant role during machining. In some cases, the absence of margin/land is also a noticeable feature, as in Fig. 1. Specifications for the drill and the work material used in the present work are given in Table 1. In the following sections, relevant material model for the epoxy taken up in the present work and modeling of material removal action of micro-drill will be presented.

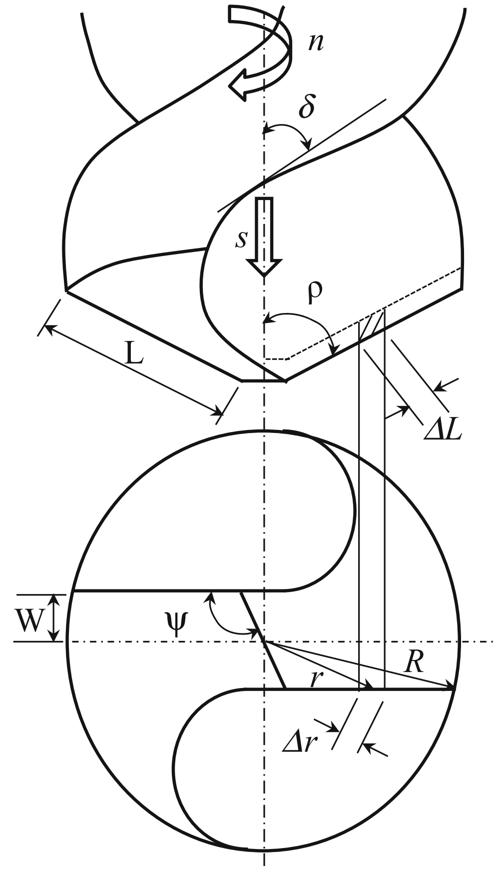

Fig. 1 Details of micro-drill used in the present work

2.1 Material model

Researchers working in metal cutting often find Johnson-Cook's material constitutive models to be very useful to predict yield strength at different strain, strain rate, and temperature [23]. However, these models do not cover polymers like epoxy. Generally, the compressive strength of the epoxy is found to be higher than its tensile strength. The epoxy specimens are often tested under compression to determine the yield characteristics. A suitable material model for the mechanical response of a solid amorphous polymer like epoxy, which is dependent on the temperature and strain rate, becomes necessary. Rio and Rodríguez [24] presented a material model for the variation of uniaxial compressive yield stress σ_y with strain rate $\dot{\varepsilon}$ and absolute temperature T as described by Richeton et al. in [25] and the equation is given as:

$$\sigma_y = \sigma_i(0) - mT + \frac{2kT}{V_a}\sinh^{-1}\left[\frac{\dot{\varepsilon}}{\dot{\varepsilon}_0 \exp\left(-\frac{\Delta H_\beta}{kT}\right)}\right]^{1/n_c} \quad (1)$$

where $\sigma_i(0)$ is the internal yield stress at 0 K, m is material constant, ΔH_β is the β activation energy, V_a is the activation

Table 1 Tool and workpiece material specifications

a. Tool specification (Walter Titex K30F)	
Tool material	WC-Co
Size, $2R$	0.5 mm
Web thickness, $2W$	0.12 mm
Helix angle, δ	24°
Point angle, 2ρ	118°
Chisel edge angle, ψ	125°
Cutting edge radius, r_e	2 μm
b. Workpiece material specification	
Plain epoxy-based plastics	
Composition	Araldite LY556 and HY951 (10:1 by weight)
Sheet size	40 mm×32 mm
Sheet thickness	2.2 mm
Fiber-reinforced epoxy-based plastics	
Fiber (size)	Glass (10 μm)
Fiber strength	Tensile, 3.40 GPa
	Shear, 300 MPa
Volume fraction	30 %
Fabric count (weave type)	32×30 (plain)
Average fabric thickness	200 μm
Sheet size	40 mm×32 mm
Sheet thickness	2.2 mm

volume, $\dot{\varepsilon}_0$ is the pre-exponential strain rate, n_c is the material parameter to characterize the cooperative movement of the chain segments, and k is the Boltzmann's constant. Richeton model parameters summarized by Río and Rodríguez [24] for the epoxy polymer are given in Table 2. The temperature in micro-drilling is taken to be in the range of 60–100 °C, which is below the glass transition temperature of the epoxy considered. From the properties of epoxy listed in different sources, it is seen that compressive strength is higher than the tensile strength, and ratio between compressive yield strength and shear strength varies from 2.5 to 3.5. In the present work, a ratio of 3 is taken to compute the shear strength (τ) of the matrix epoxy used in the mechanistic model [26].

In the above equation, value $\dot{\varepsilon}$ corresponding to different zones of deformation must be taken. The size effect in epoxy-based plastics is quite different from that in metals. Though the size effect of epoxy-based plastics has been experimentally identified through indentation method [27] and micro-compression test [28], a generalized formulation as in the case of metals is needed. In the absence of such generalized model and based on the fact that size effect is observed for indentation depths below 2 μm for different epoxies, its effect is not included in the material model as feed used in present work is 5 μm/rev and above.

2.2 Material removal action in micro-drilling

In general, material removal in drilling happens in three distinct regions, namely cutting lip (primary), chisel edge (secondary), and indentation regions. Material removal at lip and chisel edge (excluding indentation) regions is by cutting action. From literature, it is seen that phenomena associated with orthogonal cutting of plastics are observed to be similar to those in metal cutting [11, 12]. However, shearing no longer occurs along a plane when the depth of cut is as small as in micro-cutting. Therefore, applicability of thin zone models in such cases has to be justified. In a work reported by Tounsi et al. [29], the shear zone is approximated by a rectangular zone and a main shear plane along which maximum shearing occurs is identified within this rectangular zone. In the present work, main shear plane as suggested in Tounsi's model is taken as a limiting case, and all the relevant parameters are computed on the basis of thin zone model. Appropriate oblique cutting model derived from thin zone orthogonal model is used in developing mechanistic model for cutting forces in micro-drilling.

2.2.1 Cutting lip (primary) zone

Figure 1 shows cutting lip geometry for the micro-drill. It is usual to consider a radial element of width Δr at a radius of r from the drill axis which corresponds to an oblique element ΔL on the lip. The relation between Δr and ΔL is given by $\Delta r = \Delta L \sin\rho\cos\omega$ where ρ is the semi-point angle and ω is the web angle. This element is treated as an oblique cutting edge, and forces acting on it are estimated from the principles of oblique cutting. The cutting edge also introduces ploughing/rubbing effect due to the radius at the edge. Therefore, the forces acting on the chosen element for unit radial width Δr in the cutting (f_P), thrust (f_Q), and radial (f_R) directions are expressed as

$$f_P = f_{pc} t_0 + f_{pe} \tag{2a}$$

$$f_Q = f_{qc} t_0 + f_{qe} \tag{2b}$$

$$f_R = f_{rc} t_0 + f_{re} \tag{2c}$$

where f_{pc}, f_{qc}, f_{rc} are cutting force coefficients; f_{pe}, f_{qe}, f_{re} are the edge force coefficients; and t_0 is the uncut chip thickness at the lip region given by

Table 2 Richeton model parameters for the epoxy chosen [24]

Model parameters	Symbol (unit)	Value
Internal yield stress at 0 K	$\sigma_i(0)$ (MPa)	265
Material constant	m (MPa/K)	0.551
Pre-exponential strain rate	$\dot{\varepsilon}_0$ (s^{-1})	7.783×10^7
β activation energy	ΔH_β (KJ/mol)	35
Parameter characterizing cooperative movement of chain segments	n	3.514
Activation volume	V (m^3)	8.84×10^{-29}
Boltzmann's constant	k (m^2 kg/s^2 K)	1.3806503×10^{-23}

$$t_0 = \frac{s\sin\rho\cos\nu}{2} \tag{3}$$

where s is feed and ν is velocity angle.

In the present work, cutting coefficients are found from the work of Armarego and Brown [3] as

$$f_{pc} = \frac{\tau\cos\nu\cos i[\cos(\beta_n - \alpha_n) + \tan i\tan\eta\sin\beta_n]}{\sin\phi_n\cos\omega\left[\cos^2(\phi_n + \beta_n - \alpha_n) + \tan^2\eta\sin^2\beta_n\right]^{1/2}} \tag{4a}$$

$$f_{qc} = \frac{\tau\cos\nu\sin(\beta_n - \alpha_n)}{\sin\phi_n\cos\omega\left[\cos^2(\phi_n + \beta_n - \alpha_n) + \tan^2\eta\sin^2\beta_n\right]^{1/2}} \tag{4b}$$

$$f_{rc} = \frac{\tau\cos\nu\cos i[\cos(\beta_n - \alpha_n)\tan i - \tan\eta\sin\beta_n]}{\sin\phi_n\cos\omega\left[\cos^2(\phi_n + \beta_n - \alpha_n) + \tan^2\eta\sin^2\beta_n\right]^{1/2}} \tag{4c}$$

where τ is shear strength.

The edge coefficients found from the model proposed by Abdelmoneim and Scrutton [30] are given:

$$f_{pe} = \frac{\tau r_e}{\sin\rho\cos\omega}\left[\frac{2\theta_0}{\cos\theta_0} + \pi\sin\theta_0\tan\theta_0\right] \tag{5a}$$

$$f_{qe} = \frac{\tau r_e}{\sin\rho\cos\omega}\left[2\sqrt{3}\sin\theta_0\right] \tag{5b}$$

$$f_{re} = f_{pe}\sin i \tag{5c}$$

where the value of stagnation angle θ_0 is taken as 14°.

Web angle ω used in the above equations is given by

$$\omega = \sin^{-1}(W/r) \tag{6}$$

where W is the half web thickness.

Based on Stabler's rule, chip flow angle η is assumed as inclination angle i which is given by

$$i = \sin^{-1}\left(\frac{W\sin\rho}{r}\right) \tag{7}$$

The rake angle α_n is given by

$$\alpha_n = \alpha_{\text{ref}} - \nu \tag{8a}$$

where velocity angle ν is

$$\nu = \tan^{-1}(\tan\omega\cos\rho) \tag{8b}$$

and reference rake angle α_{ref} is computed for a given helix angle of the drill δ as

$$\alpha_{\text{ref}} = \tan^{-1}\left(\frac{\tan\delta\cos\omega}{\sin\rho - \tan\delta\sin\omega\cos\rho}\right) \tag{8c}$$

When the uncut chip thickness t_0 is less than a limiting value t_{lim}, the rake angle α_n gets modified [10] as

$$\alpha_n = \sin^{-1}\left(\frac{t_0 - r_e}{r_e}\right) \text{ for } t_0 < t_{\text{lim}} \tag{9}$$

where r_e is cutting edge radius and t_{lim} is the limiting value given by $t_{\text{lim}}=r_e(1+\sin\alpha_n)$. Otherwise, Eq. 8(a) is directly used.

A modified shear angle relation used by Rao and Shunmugam [23] to predict shear angle φ_n is given as:

$$\varphi_n = \frac{C - \beta_n + \alpha_n}{2} \tag{10}$$

where C is Merchant's machining constant.

The strain rate ($\dot{\varepsilon}$) on the shear plane is given by Tounsi et al. [29] as

$$\dot{\varepsilon} = \frac{2V\cos(\alpha_n)}{\sqrt{3}h\cos(\phi_n - \alpha_n)} \tag{11}$$

where V is cutting velocity (mm/s) at radius r and h is primary shear zone thickness (=t_0/2).

The thrust and tangential forces at jth element on the lip with reference to drill axis can be found from the following equations:

$$\text{Thru}_j = \left[f_{Q_j}(\cos\nu\sin\rho) - f_{R_j}(\cos i\cos\rho + \sin i\sin\nu\sin\rho)\right]\Delta r \tag{12a}$$

$$\text{Tang}_j = f_{P_j}\Delta r \tag{12b}$$

Therefore, thrust force (Thru_{lip}) and torque (Torq_{lip}) on both the lips can be computed by summing over all N elements.

$$\text{Thru}_{\text{lip}} = 2\sum_{j=1}^{j=N}\text{Thru}_j \tag{13a}$$

$$\text{Torq}_{\text{lip}} = 2\sum_{j=1}^{j=N}\text{Tang}_j r_j \tag{13b}$$

2.2.2 Chisel edge (secondary) zone—indentation zone excluded

The procedure followed for prediction of cutting forces acting on the chisel edge is similar to that described in Section 2.2.1. One portion of the chisel edge represented as C (half chisel edge length minus radius of indentation zone R_a) in Fig. 2 is divided into M elements. Elemental forces ΔF_P and ΔF_Q acting on a given element of width Δr and thickness s/2 at a distance of r from the drill axis in cutting and thrust directions can be expressed by Eq. 2(a) and 2(b). The relevant cutting force coefficients can be derived from Eq. 4 using conditions for orthogonal cutting, namely $i=\eta=\omega=\nu=0$. In the final form, Eqs. 4(a) and 4(b) appear as:

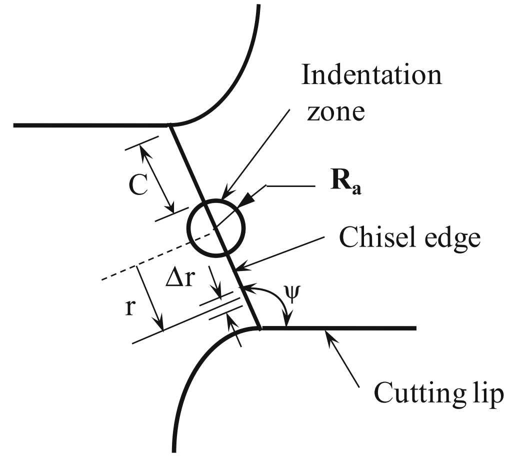

Fig. 2 Chisel edge and indentation zone

$$f_{pc} = \frac{\tau\cos(\beta_n - \alpha_n)}{\sin\phi_n\cos(\varphi_n + \beta_n - \alpha_n)} \tag{14a}$$

$$f_{qc} = \frac{\tau\sin(\beta_n - \alpha_n)}{\sin\phi_n\cos(\varphi_n + \beta_n - \alpha_n)} \tag{14b}$$

The edge force coefficients are expressed by Eqs. 5(a) and 5(b).

However, the rake angle at the element on the chisel edge must be taken according to [6]:

$$\alpha_n = \alpha_{\text{ref}} + \alpha_s \tag{15a}$$

where reference rake angle α_{ref} and feed angle α_s are, respectively, given by

$$\alpha_{\text{ref}} = -\tan^{-1}(\tan\rho\cos(\pi - \psi)) \tag{15b}$$

$$\alpha_s = \tan^{-1}\left(\frac{s}{2\pi r}\right) \tag{15c}$$

The limiting condition in Eq. 9 must be considered while taking into account the edge radius effect on rake angle in cutting.

Since the feed and cutting velocities are also comparable in this zone, velocity according to the next equation must be taken to compute shear strain $\dot{\varepsilon}$ using Eq. 11.

$$V = \frac{n}{60}\sqrt{s^2 + (2\pi r)^2} \tag{16}$$

The thrust and tangential forces at kth element on the chisel edge with reference to drill axis can be found from the following equations

$$\text{Thru}_k = \left[f_{Q_k}\right]\Delta r \tag{17a}$$

$$\text{Tang}_k = \left[f_{P_k}\right]\Delta r \tag{17b}$$

The thrust force (Thru_{chi}) and torque (Torq_{chi}) due to chisel edge cutting can be found by summing over all M elements and multiplying by 2 to account for two portions of chisel edge on either side of the indentation zone.

$$\text{Thru}_{\text{chi}} = 2\sum_{k=1}^{k=M}\text{Thru}_k \tag{18a}$$

$$\text{Torq}_{\text{chi}} = 2\sum_{k=1}^{k=M}\text{Tang}_k r_k \tag{18b}$$

2.2.3 Indentation zone

In the indentation zone, the velocity is near zero, and material in this zone is pushed backward due to compressive stress. This zone cannot be neglected in micro-drilling, as its contribution to the drilling forces is appreciable [8, 20]. The portion of the chisel edge at this zone is considered to be a rigid wedge having a semi-angle of α_n given by Eq. 13 in which feed angle α_s is zero. Using slip-line solution provided by Kachanov [31], normal force acting on the wedge is determined. From the normal force, thrust force and torque at the indentation zone can be found as

$$\text{Thru}_{\text{ind}} = \frac{8\tau(1+\phi)sR_a\sin\alpha_n}{\cos\alpha_n - \sin(\alpha_n-\phi)} \tag{19a}$$

$$\text{Torq}_{\text{ind}} = \frac{4\tau(1+\phi)sR_a{}^2\cos\alpha_n}{\cos\alpha_n - \sin(\alpha_n-\phi)} \tag{19b}$$

where angle ϕ is found out iteratively from the relation,

$$2\alpha_n = \phi + \cos^{-1}\left\{\tan\left(\frac{\pi}{4}-\frac{\phi}{2}\right)\right\} \tag{19c}$$

Radius of the indentation zone is obtained from the relation involving feed s and semi-point angle ρ as [32]:

$$R_a = \frac{s}{4\tan\left(\frac{\pi}{2}-\rho\right)} \tag{20}$$

2.2.4 Total forces acting on a micro-drill

Total thrust force (Thru) and torque (Torq) acting on the drill can be found by adding the values at all three zones.

$$\text{Thru} = \text{Thru}_{\text{lip}} + \text{Thru}_{\text{chi}} + \text{Thru}_{\text{ind}} \tag{21a}$$

$$\text{Torq} = \text{Torq}_{\text{lip}} + \text{Torq}_{\text{chi}} + \text{Torq}_{\text{ind}} \tag{21b}$$

3 Experimental validation

For validating the model developed in the previous section, micro-drilling experiments are conducted on an in-house developed miniaturize machine tool (MMT) having a high-speed spindle with a speed range of 5,000 to 100,000 rpm and a runout of less than 1 μm [33]. The spindle speed is controlled through the frequency converter which allows infinitely variable speed within the range. A piezo-electric dynamometer Kistler MiniDyn 9256C2 with a minimum resolution of 0.002 N and Kistler multi-channel charge amplifier Type 5070A are used to measure thrust force and torque during micro-drilling.

The specimen for the experimental work for the first set of experiments is a rectangular sheet of 2.25 mm thickness made out of matrix material and having a dimension 40×32 mm. The matrix material is made of bifunctional diglycidyl ether of bisphenol A (DGEBA)-type epoxy resin (LY556) and triethylene teramine (TETA)-type curing agent (HY951) in the ratio of 10:1 by weight. The prepared matrix mixture is cured at room temperature for 24 h and post-cured for 2 h at 150 °C. The glass transition temperature (Tg) is identified as 115 °C. The second set of experiments is carried out on the GRP sheet of the same size having the same matrix and six layers of woven glass 32×30 (count) fabric with a volume fraction of 30 % (Table 1). The average thickness of each fabric layer is about 200 μm [21]. The specimen is clamped on a special fixture which is turn mounted centrally on the dynamometer so as to avoid any adverse moments during machining, with uniform torque on the clamping screws. The entire setup is placed on a vibration isolation table to avoid any vibration transmitted from the surrounding. Table 3 gives the experimental plan involving full factorial design with speed and feed at three levels. A solid carbide drill of

Table 3 Average thrust and torque measured during micro-drilling

Sl. no.	Speed, *n* (rpm)	Feed, *s* 10^{-3} (mm//rev)	Plain		GFR	
			Thru (N)	Torq (N mm)	Thru (N)	Torq (N mm)
1	20,000	5	0.5984	0.2967	0.9299	0.3685
2	30,000	5	0.5657	0.2484	0.9910	0.3316
3	40,000	5	0.5442	0.2222	0.9036	0.2930
4	20,000	10	0.9207	0.3278	1.4565	0.4633
5	30,000	10	0.8699	0.3184	1.3535	0.4074
6	40,000	10	0.8252	0.2516	1.3436	0.3417
7	20,000	15	1.2107	0.4365	1.8636	0.7000
8	30,000	15	1.1180	0.3978	1.8782	0.5618
9	40,000	15	1.0044	0.3225	1.7085	0.5505

0.5-mm diameter with specification given in Table 1a is used. The levels of speed (20,000, 30,000, and 40,000 rpm) and feed (5, 10, and 15 μm/rev) are chosen based on recommendations in literature and micro-drill manufacturer's catalogue [21, 22]. For each condition, a blind hole of 0.6 mm is drilled directly (without pecking cycle) to capture the variation in thrust and torque values. Figure 3 shows typical thrust and torque signals obtained during micro-drilling experiment, corresponding to the conditions specified in the first row of Table 3.

4 Results and discussion

It is seen from Fig. 3 that full engagement happens after entry of the drill point, and a dwell of 0.5 s is allowed before withdrawing the drill. These zones are marked on the plots for better visualization of variation of forces during different phases of drilling. In an earlier work reported by the authors [21, 22], maximum values of thrust and torque acting on the drill are taken for analysis as they are considered critical in controlling the drill breakage. It is observed that such maxima can occur anywhere during the drilling cycle. Since the mechanistic model proposed in the present work predicts thrust and torque during full engagement phase, it is considered appropriate to take the average values of thrust and torque in the full engagement zone and compare with the predicted values. Based on a minimum of three trials carried out for the specified drilling conditions, the average thrust and torque values are given in Table 3.

4.1 Plain epoxy sheet

For predicting the drilling forces using the mechanistic model, appropriate value of C has to be used in Eq. 8. In orthogonal machining of plastics, Rao et al. [11] identified C to be 1.57 (90 deg) and discussed the role of friction in determining the forces. In the present work, $(C-\beta_n)$ is taken as a single parameter for prediction and analysis of thrust and torque at lip and chisel cutting edges. The predicted thrust force (Thru) and torque (Torq) are given in Table 4 with $(C-\beta_n)=1.29$ for

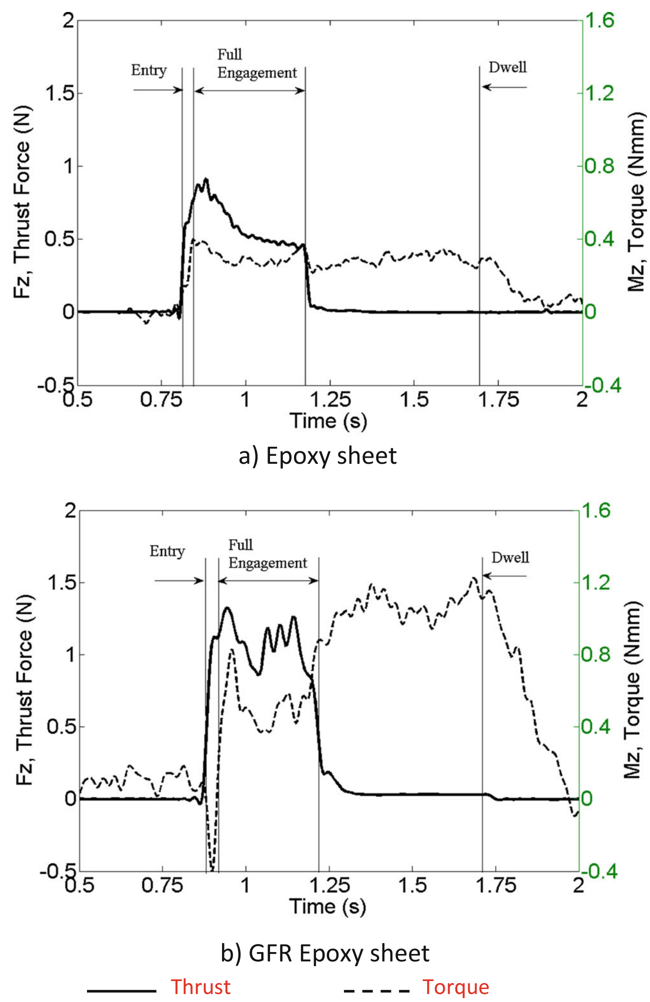

Fig. 3 Typical plots showing variation in thrust and torque during micro-drilling (speed, 20,000 rpm; feed, 5 μm/rev). **a** Epoxy sheet, **b** GFR epoxy sheet

Table 4 Comparison of predicted thrust and torque with measured values

Sl no.	Thru (N)				Torq (N mm)			
	Experimental		Predicted	% Deviation	Experimental		Predicted	% Deviation
	Measured	Adjusted			Measured	Adjusted		
a. Plain epoxy-based plastic [$Thru_{swr}$=0.107–1.42(10^{-4})V_R+8.87s; $Torq_{swr}$=0.273–1.62(10^{-4})V_R+6.55s]								
1	0.5984	0.5214	0.5485	−5.20	0.2967	0.0758	0.0721	4.85
2	0.5657	0.5259	0.5392	−2.53	0.2484	0.0699	0.0714	−2.17
3	0.5442	0.5416	0.5260	2.87	0.2222	0.0861	0.0703	18.35
4	0.9207	0.7994	0.7906	1.09	0.3278	0.0741	0.1004	−35.45
5	0.8699	0.7857	0.7714	1.82	0.3184	0.1071	0.0991	7.50
6	0.8252	0.7782	0.7464	4.09	0.2516	0.0827	0.0970	−17.23
7	1.2107	1.0450	1.0230	2.11	0.4365	0.1501	0.1382	7.91
8	1.1180	0.9895	0.9933	−0.39	0.3978	0.1538	0.1360	11.56
9	1.0044	0.9131	0.9561	−4.71	0.3225	0.1209	0.1327	−9.76
Avg. abs. deviation (%)				2.76	Avg. abs. deviation (%)			12.75
b. Glass fiber-reinforced epoxy-based plastics [$Thru_{swr}$=0.219–1.28(10^{-4})V_R–1.09s; $Torq_{swr}$=0.295–2.16(10^{-4})V_R+16.8s]								
1	0.9299	0.7834	0.8380	−6.97	0.3685	0.1026	0.1027	−0.10
2	0.9910	0.8780	0.8315	5.29	0.3316	0.1222	0.1023	16.32
3	0.9036	0.8241	0.8222	0.23	0.2930	0.1402	0.1015	27.60
4	1.4565	1.3154	1.2862	2.22	0.4633	0.1134	0.1487	−31.13
5	1.3535	1.2459	1.2727	−2.15	0.4074	0.1140	0.1477	−29.51
6	1.3436	1.2695	1.2552	1.13	0.3417	0.1049	0.1463	−39.47
7	1.8636	1.7280	1.7392	−0.65	0.7000	0.2661	0.2086	21.60
8	1.8782	1.7761	1.7185	3.24	0.5618	0.1844	0.2070	−12.23
9	1.7085	1.6399	1.6924	−3.20	0.5505	0.2297	0.2047	10.88
Avg. abs. deviation (%)				2.79	Avg. abs. deviation (%)			20.98

% deviation=100(Exp.−Pred.)/Exp.

plain epoxy sheet considered in this work. From Fig. 3a, it can be seen that thrust exists during the dwell, whereas torque exists during the dwell as well as withdrawal phases. This clearly shows that micro-drill rubs against the side wall of the drilled holes, and the rubbing has a different effect on the measured thrust and torque. Since mechanistic models proposed in the present work predict the thrust and torque without the effect of side wall rubbing, its effect is removed from the measured values according to Eq. 22.

$$Thru_{swr} = k_{f1} + k_{f2}V_R + k_{f3}s \quad (22a)$$

$$Torq_{swr} = k_{m1} + k_{m2}V_R + k_{m3}s \quad (22b)$$

where V_R is the velocity in millimeters per second at the periphery of the drill (R=0.25 mm) and s is feed in millimeters per revolution. The coefficients k_{f1}, k_{f2}, k_{f3} and k_{m1}, k_{m2}, k_{m3} obtained by regression are also given in Table 4. The values of $Thru_{swr}$ and $Torq_{swr}$ are subtracted from the measured values and given as adjusted values in Table 4. The material model given by Eq. 1 and relevant details from Table 2 are used in the mechanistic model to predict the thrust and torque during micro-drilling. The deviations from the predicted values are tabulated, and the average absolute deviations are obtained as 2.76 and 12.75 %, respectively, for thrust force and torque. Higher percentage of deviation for the torque is due to the larger scatter in the measured values of torque in comparison with the thrust measured [21].

4.2 Glass-reinforced epoxy sheet

Glass fiber fabric used as reinforcement is a plain woven type with a distinct checkerboard pattern formed by lengthwise warp yarn passing over, under, over, and under the crosswise filling yarn. Each yarn consists of several fibers, and woven fabric is approximately 200 μm thick (Table 1). Unlike orthogonal edge cutting of unidirectional fiber-reinforced laminate, micro-drilling is carried out on the sheet surface. Hence, the cutting edges of the micro-drill cut through the fibers at different orientations. In comparison with matrix material, the glass fibers exhibit lower compressive strength than tensile strength. The shear strength of fiber is much lower than the compressive strength [34]. In the present work, it is considered appropriate to model the GRP as an equivalent homogeneous material for the prediction of average drilling forces using the mechanistic model. Since this is a first attempt to model the behavior of GRP in micro-cutting, a simplified material model using rule of mixtures is used to arrive at the equivalent shear strength.

The shear strength of glass-reinforced epoxy is derived using the following relation:

$$\tau_{comp} = \tau_{fib} v_{fib} + \tau_{mat} v_{mat} \tag{22}$$

where τ_{comp}, τ_{fib}, and τ_{mat} represent shear strength of composites, fiber, and matrix, respectively. Volume fraction of fiber and matrix in the composites are represented by v_{fib} and v_{mat}, respectively. In the present work, volume fraction of fiber in the laminate is 30 % and its shear strength is 300 MPa as given in Table 1.

Average thrust and torque values are computed following the same procedure that has been outlined for the plain epoxy sheets, and these measured average values are given in Table 3. The average absolute deviations are obtained as 2.79 and 20.98 %, respectively, for thrust force and torque, as given in Table 4. In case of GRP sheets, the average absolute deviation is higher than that obtained for plain sheets, as fibers present in the matrix give rise to greater fluctuations in the force signals and hence higher degree of scatter.

5 Conclusions

It is seen from the literature that many researchers deal with statistical models for cutting forces in machining of fiber-reinforced plastics, and a few models based on finite element analysis have been reported. Though mechanistic models of cutting forces are reported for metal machining, such an approach for fiber-reinforced plastics has not been attempted. As a first attempt, it is established that it is possible to develop mechanistic models of drilling forces in micro-drilling for both plain and glass-reinforced epoxy sheets.

The mechanistic model is validated with experimental results. During the validation, it is observed that rubbing of the micro-drill with side wall of the drilled hole influences the thrust and torque during micro-drilling. When this effect is taken into account, the average absolute deviations in prediction of drilling thrust and torque are obtained as 2.76 and 12.75 %, respectively, in micro-drilling of plain epoxy sheets. In case of GRP sheets, these values are 2.79 and 20.98 % for thrust and torque, respectively. Though the prediction error of 20.98 % is higher for torque obtained in micro-drilling of GRP, it is reasonable considering the non-homogenous nature of glass fiber reinforcement in the composites.

Though the proposed model is developed for micro-drilling of plain and glass-reinforced epoxy sheets, it is equally applicable to macro-drilling of plain and fiber-reinforced plastics with minor changes.

Acknowledgments The authors thank the Department of Science and Technology (DST) and Aeronautical Research and Development Board (ARDB), Government of India, for the project grants from which the machines and instruments used for the present investigation have been procured.

References

1. Chen WS, Ehmann KF (1994) An experimental investigation on the wear and performance of micro-drills. ASME Cent Res Tech Dev (CRTD) 30:145–157
2. Oxford CJ (1955) On the drilling of metals I: basic mechanics of the process. Trans ASME 77:103–114
3. Armarego E, Brown R (1969) The machining of metals. Prentice-Hall, Englewood Cliffs
4. Wang J, Zhang Q (2008) A study of high-performance plane rake faced twist drills. Part II: predictive force models. Int J Mach Tools Manuf 48:1286–1295
5. Rubenstein C (1991) The torque and thrust force in twist drilling—II. Comparison of experimental observations with deductions from theory. Int J Mach Tools Manuf 31:491–504
6. Armarego E, Cheng C (1972) Drilling with flat rake face and conventional twist drills—I. Theoretical investigation. Int J Mach Tool Des Res 12:17–35
7. Armarego E, Wright J (1984) Predictive models for drilling thrust and torques—a comparison of three flank configurations. Ann CIRP Manuf Technol 33:5–10
8. Gong Y, Ehmann KF (2001) Mechanistic model for dynamic forces in micro-drilling, *Proc 2001 ASME Int Mech Eng Cong Expo*, New York, 1-10
9. Shaw MC (2003) The size effect in metal cutting. Sadhana 28:875–896
10. Bissacco G, Hansen HN, Slunsky J (2008) Modelling the cutting edge radius size effect for force prediction in micro milling. Ann CIRP Manuf Technol 57:113–116
11. Rao UM, Cumming JD, Thomsen EG (1964) Some observations on the mechanics of orthogonal cutting of Derlin and Zytel plastics. J Eng Ind 117–121
12. Kobayashi A (1967) Machining of plastics. McGraw-Hill, New York
13. Arola D, Ramulu M (1997) Orthogonal cutting of fibre-reinforced composites: a finite element analysis. Int J Mech Sci 39:597–613
14. Arola D, Sultan MB, Ramulu M (2002) Finite element modeling of edge trimming fibre-reinforced plastics. Trans ASME J Manuf Sci Eng 124:32–41
15. Venu Gopala Rao G, Mahajan P, Bhatnagar N (2007) Micro-mechanical modeling of machining of FRP composites—cutting force analysis. Comp Sci Technol 67:579–593
16. Khashaba UA (2004) Delamination in drilling GFR-thermoset composites. Comp Struct 63:313–327

17. Khashaba UA (2013) Drilling of polymer matrix composites: a review. J Comp Mater 47(15):1817–1832
18. Davim JP, Reis P, Antonio CC (2004) Experimental study of drilling glass fiber reinforced plastics (GFRP) manufactured by hand lay-up. Comp Sci Technol 64:289–297
19. Singh I, Bhatnagar N, Viswanath P (2008) Drilling of uni-directional glass fiber reinforced plastics: experimental and finite element study. Mater Des 29:546–553
20. Chandrasekharan V, Kapoor S, DeVor R (1995) A mechanistic approach to predicting the cutting forces in drilling: with application to fiber-reinforced composite materials. Trans ASME J Eng Ind 117:559–570
21. Rahamathullah I, Shunmugam MS (2011) Thrust and torque analyses for different strategies adapted in micro-drilling of glass-fibre-reinforced plastics. Proc IMechE Part B: J Eng Manuf 225:505–519
22. Rahamathullah I, Shunmugam MS (2013) Analyses of forces and hole quality in micro-drilling of carbon fabric laminate composites. J Comp Mater 47(9):1129–1140
23. Rao S, Shunmugam MS (2012) Analytical modeling of micro end-milling forces with edge radius and material strengthening effects. Mach Sci Technol 16(2):205–227
24. Río GT, Rodríguez J (2012) Compression yielding of epoxy: Strain rate and temperature effect. Mater Des 35:369–373
25. Richeton J, Ahzi S, Daridon L, Rémond Y (2005) A formulation of the cooperative model for the yield stress of amorphous polymers for a wide range of strain rates and temperatures. Polymer 46:6035–6043
26. Kaw AK (2006) *Mechanics of composite materials* (2nd Edition). CRC, Florida
27. Han C-S, Nikolov S (2007) Indentation size effects in polymers and related rotation gradients. J Mater Res 22(6):1662–1672
28. Wang S, Yang Y, Zhou LM, Mai Y-W (2012) Size effect in microcompression of epoxy micropillars. J Mater Sci 47(16):6047–6055
29. Tounsi N, Vincenti J, Otho A, Elbestawi M (2002) From the basic mechanics of orthogonal metal cutting toward the identification of the constitutive equation. Int J Mach Tools Manuf 42:1373–1383
30. Abdelmoneim ME, Scrutton RF (1974) Tool edge roundness and stable build-up formation in finish machining. Trans ASME 96: 1258–1267
31. Kachanov LM (1971) Foundations of the theory of plasticity. North Holland, Amsterdam
32. Mauch CA, Lauderbaugh LK (1990) Modeling the drilling process—an analytical model to predict thrust force and torque. Proc Comput Model Simul Manuf Process ASME PED 48:59–65
33. Srinivasa YV, Shunmugam MS (2009) Development and performance evaluation of miniaturized machine tool (MMT) system. Int J Nanomanufacturing 3(1/2):133–158
34. Barbero EJ (2010) Introduction to composite materials design, 2nd edn. CRC, Philadelphia